Three-dimensional electron momentum densities of graphite and fullerene: a comparison

1999 J. Phys.: Condens. Matter 11 3933

(http://iopscience.iop.org/0953-8984/11/19/312)

J. Phys.: Condens. Matter **11** (1999) 3933–3942. Printed in the UK PII: S0953-8984(99)00427-0

Three-dimensional electron momentum densities of graphite and fullerene: a comparison

C Metz†, Th Tschentscher†¶, P Suortti†, A S Kheifets‡, D R Lun‡, T Sattler§, J R Schneider§ and F Bell‖

† European Synchrotron Radiation Facility (ESRF), BP 220, F-38043 Grenoble, France
‡ Atomic and Molecular Physics Laboratory, Research School of Physical Sciences and Engineering, The Australian National University, Canberra, ACT 0200, Australia
§ Hamburger Synchrotronstrahlungslabor (HASYLAB) at Deutsches Elektronen-Synchrotron (DESY), Notkestrasse 85, D-22603 Hamburg, Germany
‖ Sektion Physik, Universität München, Am Coulombwall 1, D-85748 Garching, Germany

Received 29 December 1998, in final form 26 March 1999

Abstract. We report on the three-dimensional electron momentum densities (EMD) of graphite and fullerene obtained by a so-called $(\gamma, e\gamma)$ experiment, i.e. the coincident detection of an inelastically scattered hard x-ray photon with its recoil electron. A monochromatized flux of 10^{12} photons s^{-1} at 150 keV from the high-energy x-ray wiggler beamline of the ESRF was directed onto thin graphite or fullerene targets. Comparison with a pseudopotential and a full-potential linear muffin-tin orbital calculation in the case of graphite is made. Inclusion of electron correlation via the Lam–Platzman correction is discussed. The experimental EMD of C_{60} shows stronger electron delocalization in the 'buckyball' compared to graphite, which is supported by theory.

1. Introduction

Traditionally, Compton scattering has been used to characterize the electron momentum density (EMD) of valence electrons in solids [1]. The double-differential cross section describing the energy and angular distribution of inelastically scattered x-rays is proportional to the so-called Compton profile which is defined as a twofold integration over the EMD $\rho(\boldsymbol{p})$:

$$J(p_z) = \int\int \rho(p_x, p_y, p_z)\, \mathrm{d}p_x\, \mathrm{d}p_y \tag{1}$$

where p_z is a function of both the scattered photon energy and the scattering angle. The integration results from the lack of information about the momentum distribution of the recoiling electrons. It can be avoided if the recoil electron is measured simultaneously with the scattered photon. The corresponding triple-differential cross section for such a $(\gamma, e\gamma)$ experiment is proportional to the EMD itself. Since integration averages over large volumes in momentum space, experiments which avoid this are desirable. If the momenta of the primary and scattered photon in addition to that of the recoiling electron are fixed experimentally, the initial electron momentum can be reconstructed in a unique way. The accuracy of a $(\gamma, e\gamma)$ experiment depends on the possibility of measuring the recoil momentum undisturbed by multiple elastic scattering within the target. Since the mean free path of elastic scattering

¶ Now at: HASYLAB (DESY), Hamburg, Germany.

0953-8984/99/193933+10$19.50

for 50 keV electrons in carbon is only about 85 nm [2], self-supporting targets are required which are as thin as possible. Alternatives to $(\gamma, e\gamma)$ experiments are two-dimensional angular correlations of annihilation radiation (2D-ACAR) [3]—which measure the momentum density weighted by the positron wavefunction—and (e, 2e) experiments, where the projectile is an electron. A recent review article about this kind of momentum spectroscopy focuses especially on the electronic structures of different forms of solid carbon [4].

In the following we will describe experimental results for the EMDs of graphite and C_{60} which will be compared to theories based on a pseudopotential or linear muffin-tin orbital calculation.

2. Experiment

The experiment was performed at the High Energy X-ray Scattering beamline ID15A of the ESRF [5]. The photons from an asymmetric wiggler with seven periods and strong poles of 1.8 T at a 20.3 mm gap were monochromatized by a (220) bent Si crystal yielding 150 keV photons ($\Delta\omega = 0.74$ keV FWHM) with an intensity of roughly 10^{12} photons s^{-1}. They entered an evacuated target chamber with an externally mounted intrinsic Ge diode at a scattering angle of 140°. At this angle the scattered photon energy was about 100 keV. The 50 keV recoil electrons were measured with a two-dimensional position-sensitive detector (PSD) consisting of 16×16 individual photodiodes. Figure 1 shows the arrangement of the initial and scattered photon momenta $\boldsymbol{k}$ and $\boldsymbol{k}'$, and the recoil momentum $\boldsymbol{p}'$ from which the initial electron momentum $\boldsymbol{p} = \boldsymbol{k}' + \boldsymbol{p}' - \boldsymbol{k}$ is obtained. The centre of the PSD was placed in the direction of $\boldsymbol{q}_0$, the momentum-transfer vector for the scattering of photons by electrons at rest. The surface normal of the target foils was parallel to $\boldsymbol{q}_0$. A momentum transfer of $q_0 = 63$ au guaranteed the validity of the impulse approximation. Detailed Monte Carlo (MC) calculations of the momentum resolution of the $(\gamma, e\gamma)$ spectrometer included the correlated scattering due to the triple-differential cross section, the solid angle and energy resolution of the Ge diode, the energy width of the primary beam and the beam spot at the target. The variance vector for the momentum uncertainty in the three Cartesian directions of $\boldsymbol{p} = (p_x, p_y, p_z)$ was $\boldsymbol{\sigma}_p = (0.18, 0.43, 0.20)$ au. Here, p_z is parallel to the momentum transfer $\boldsymbol{q}_0$, p_x lies in the $(\boldsymbol{k}, \boldsymbol{k}')$ scattering plane and p_y is perpendicular to it. Emission patterns of the recoiling electrons were analysed by the PSD with a granularity of about 0.14 au in the p_x-direction and 0.28 au in the p_y-direction. Thus the variance in the p_y-direction extended over two pixels and in the p_x-direction over one pixel. Time correlation spectra showed very few chance coincidences, which nevertheless were taken into account. The overall coincidence rate was about 2 Hz. A total of 4×10^5 coincidence events were accumulated for each of the two targets. One of them was a 5 μg cm^{-2} thin graphite foil made by laser plasma ablation. The ejected carbon atoms were deposited on a thin betaine film which had a fine crystalline-like structure

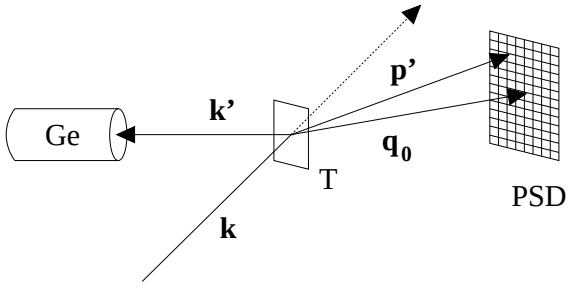

Figure 1. The experimental set-up: Ge: Ge diode; T: target; PSD: position-sensitive electron detector.

that acted as a replica for the graphite film and guaranteed a high mechanical stability. Finally, the betaine film was dissolved in water and the foil mounted on an aluminium frame. Electron diffraction revealed graphite-like Debye–Scherrer rings indicating isotropically distributed crystals with no texture [6]. The other target was 23 μg cm^{-2} purified C_{60} evaporated at 500 °C on a 3 μg cm^{-2} graphite carbon backing. With mass densities of 2.3 g cm^{-3} for graphite and 1.7 g cm^{-3} for fullerite one obtains for the graphite target a thickness of 22 nm and for the other target 130 nm fullerite on a backing of 13 nm graphite. Historically, the first C_{60} clusters were also made by laser vaporization but followed by cooling in a helium supersonic jet [7]. We stress that in the following, neither the multiple-scattering calculation nor the evaluation of composite EMDs for fullerene on a graphite backing depend on the knowledge of the mass density.

3. Theory

We will compare experimental EMDs with those obtained from theory. We have simulated the whole experiment by a master MC code which, in addition to the experimental resolution described in section 2, incorporated the theoretical EMD, the elastic multiple scattering of the emerging electrons and the granularity of the PSD. The treatment of multiple scattering follows closely that of Salvat *et al* [8]. Finally the MC result has been normalized to the total number of experimental coincident events within an integration volume with $p_x = \pm 1.4$ au, $p_y = \pm 2.5$ au and $p_z = \pm 6.0$ au. Though both targets should generate isotropic scattering, we cannot integrate the experimental results spherically over the momentum since the momentum resolutions for the Cartesian components of $\boldsymbol{p}$ are different and multiple scattering influences the p_x- and p_y-components more strongly than those in the p_z-direction. We thus present in the following specific cuts through the EMD while comparing with theory. The theoretical distributions are based on either an empirical pseudopotential (PP) method [9] with potential parameters from Reed *et al* [10] or the full-potential linear muffin-tin orbital (FP-LMTO) method [11]. Both calculations were performed within the general scheme of density functional theory (DFT). In the FP-LMTO method, a number of non-overlapping muffin-tin spheres are introduced; the potential is expanded in spherical harmonics inside the spheres and Fourier transformed in the interstitial region. It is thought that this treatment is superior to the LMTO method within the atomic sphere approximation (ASA) [12]. In addition to the problem of overlapping Wigner–Seitz (WS) spheres for the calculation of EMDs [13], the rather open graphite structure yields discontinuities of the potential at the WS radius which forces the introduction of fictitious empty spheres at interstitial sites [14, 15]. All this is avoided in the FP-LMTO method.

Both theories hold for the valence electrons in graphite and have been spherically averaged for comparison with experiment. In the case of C_{60} a molecular calculation based on the DFT was performed in the local density approximation (LDA) with a Vosko–Wilk–Nusair local potential [16]. Both experimental Compton profile measurements and theory for fullerene [17] have shown that the solid-state effect of macroscopic C_{60} targets (fullerite) is extremely weak and this has therefore been neglected. In all cases a $1s^2$ atomic core from Roothaan–Hartree–Fock wavefunctions has been added [18].

It is common to all of the calculations cited above that the electron–electron interaction is approximated by a more or less refined version of the exchange–correlation potential in the effective single-particle Schrödinger equation. But it has also been known for a while that EMDs obtained from the Kohn–Sham equations of DFT are inaccurate due to a change of the occupation number density $\Delta N = N^{ia} - N^{f}$ [19–21]. (N^{ia} and N^{f} are the properly normalized occupation numbers for a homogeneous interacting and non-interacting free-

electron gas, respectively.) While N^f is different from zero only below the Fermi momentum p_F, N^{ia} also populates states above p_F. As discussed first by Lundqvist [22], a single-particle hole couples to the plasmon, resulting in a quasiparticle called a plasmaron whose lifetime broadening in the vicinity of the Fermi momentum yields tails above p_F. The resulting correction $\Delta\rho_{LP}$ to the EMD [19, 23]

$$\Delta\rho_{LP}(p) = \frac{1}{4}\int_V \rho(\boldsymbol{r})\,\Delta N[\rho(\boldsymbol{r})]\,\mathrm{d}^3\boldsymbol{r} \tag{2}$$

accounts for electron correlation. $\Delta\rho_{LP}(p)$ is the so-called Lam–Platzman correction. For the electron density $\rho(\boldsymbol{r})$ we used the valence density determined from x-ray diffraction data obtained for natural single crystals of graphite [24] supplemented by the $1s^2$ core density [18]. The factor 1/4 in equation (2) results from the fact that the integration has been extended over the volume V of the unit cell of graphite which contains four carbon atoms. The occupation number density N^{ia} of the interacting electron gas depends both on the Fermi momentum p_F and the renormalization constant Z which is a measure of the spectral weight of the plasmaron [25]. For the calculation of the correction term $\Delta\rho_{LP}$, both depend on the average electron–electron spacing $r_s = (3/(4\pi\rho(\boldsymbol{r}))^{1/3}$: $p_F = (9\pi/4)^{1/3}r_s^{-1}$, and for $Z = Z(r_s)$ we used equation (36*a*) of Farid *et al* [26] in connection with an analytical representation of N^{ia} (equation (37*a*)). Figure 2 shows $\Delta\rho_{LP}(\boldsymbol{p})$. At $p = 0$ the correction $\Delta\rho_{LP}(0) = -1.2 \times 10^{-2}$ au^{-3} amounts to 3.5% of the graphite EMD. In order to get an impression of the relative strength of this correction in comparison with that for metals, we have calculated $\Delta\rho_{LP}(0)$ for the constant valence electron density in some representative metals. For this case one obtains $\Delta\rho_{LP}(0) = \Delta N(0)\,\Omega/(4\pi^3)$ where $\Delta N(0)$ is the difference between the occupation number densities at zero momentum and Ω is the atomic volume. Using the simple approximation $\Delta N(0) = -9(1-Z)/64$ [27] we have calculated $\Delta\rho_{LP}(0)$. The results are shown in table 1.

To obtain r_s we have used the valence electron density ρ_{out} of Moruzzi *et al* [28]. Compared to the value for graphite $\Delta\rho_{LP}(0) = -1.2 \times 10^{-2}$ au^{-3} (see figure 2), the LP correction for

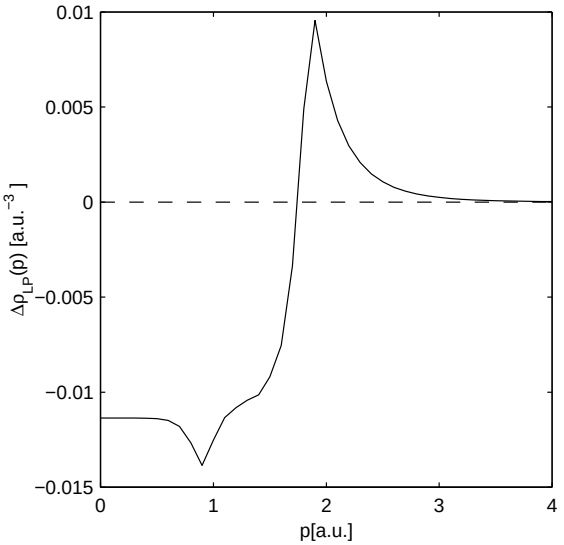

Figure 2. The Lam–Platzman correction $\Delta\rho_{LP}$ for graphite and fullerene as a function of the electron momentum p.

Table 1. Values for the Lam–Platzman correction to the momentum density $\rho(0)$ and Compton profile $J(0)$ for different metals. The parameters for the Wigner–Seitz radius r_s and the atomic volume Ω have been taken from reference [28] and for the renormalization constant Z from reference [26].

	r_s (au)	Z	Ω (au^{-3})	$\Delta\rho_{LP}(0) \times 10^2$ (au^{-3})	$\Delta J_{LP}(0) \times 10^2$ (au^{-1})
Li	3.07	0.696	132	−4.6	−3.3
Be	1.85	0.780	53	−1.3	−2.6
Na	3.67	0.663	228	−8.7	−4.4
Al	2.12	0.759	110	−3.0	−4.6
Cu	1.95	0.772	77	−2.0	−3.6

metals seems in general to be considerably larger. In addition we note that one obtains the LP correction for Compton profiles $\Delta J_{LP}(0)$ at $p_z = 0$ if $\Delta N(0)$ is replaced by

$$\Delta J(0) = -9\left(\frac{\pi}{12}\right)^{5/3}(1 - Z)r_s^{-2}.$$

The corresponding values $\Delta J_{LP}(0)$ are also shown in table 1. Except for sodium, the calculated values for $\Delta\rho_{LP}(0)$ agree reasonably well with those given by Papanicolaou *et al* [29]. Comparing $\Delta\rho_{LP}(0)$ and $\Delta J_{LP}(0)$ it is evident that the LP correction for EMDs is more sensitive to the specific material than that for Compton profiles. This is mainly due to a compensating effect: while an increasing r_s lets Z deviate more strongly from unity, the r_s^{-2}-dependence of $\Delta J_{LP}(0)$ reduces the LP correction. It even compensates for the influence of the atomic volume Ω, which is quite large for rather open structures (bcc) like those of the alkali metals.

The difference $\Delta N(0)$ of the occupation number densities becomes larger with decreasing electron density $\rho(\boldsymbol{r})$. Since the average kinetic energy T of the electrons increases as the square of their average inverse spacing ($T \propto p_F^2 \propto r_s^{-2}$), while their Coulomb energy increases only $\propto r_s^{-1}$, an electron gas behaves more 'freely' with decreasing r_s, i.e. increasing $\rho(\boldsymbol{r})$ [30]. It is for this reason that we have used the experimentally determined electron density [24] in order to make the description, especially that for regions of low density, as accurate as possible. Since the electron density of fullerene is close to that of graphite—the 'double' and 'single' carbon bond lengths in C_{60} are 1.391 Å and 1.455 Å, and thus very similar to the in-plane bonding distance of 1.421 Å in graphite—we have applied the same correction to fullerene.

4. Experimental results and discussion

In figure 3 theoretical momentum densities which have been spherically averaged are plotted, i.e. the pseudopotential calculation [9] and the FP-LMTO approximation in the case of graphite and the molecular EMD for C_{60} [16]. In the latter case, $\rho(\boldsymbol{p})$ has also been normalized to six electrons. The Lam–Platzman correction $\Delta\rho_{LP}$ has been added to all three EMDs. For comparison with experiment, theoretical data have been used in the MC simulation of the experiment as described in section 2. In figure 4 one-dimensional cuts through the 3D-EMD are shown in comparison with theory. Figure 4(a) applies to $\rho(p_x, 0, 0)$, figure 4(b) to $\rho(0, p_y, 0)$ and figure 4(c) to $\rho(0, 0, p_z)$. Though the target is spherically symmetric, both the momentum resolution and multiple scattering influence the EMD for the given directions differently. Thus, if an isotropic theory describes the data correctly, this is an indirect indication that our MC simulation works appropriately. The solid curves in figure 4 are the FP-LMTO results and the broken curves those from the pseudopotential (PP) calculation. It is evident that the PP

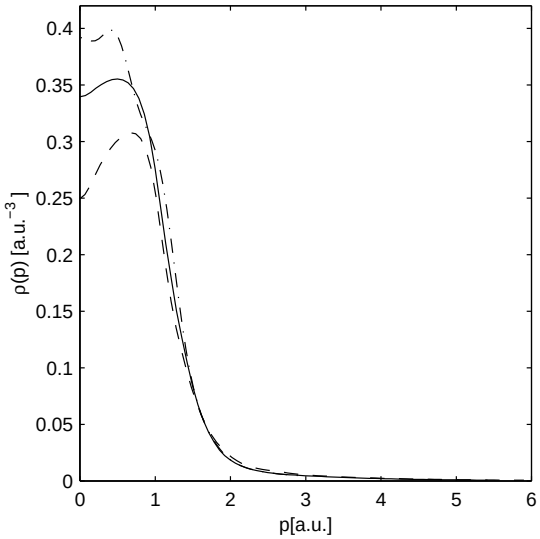

Figure 3. Spherically averaged theoretical EMDs for graphite, i.e. the pseudopotential (dashed curve) or FP-LMTO calculation (solid curve), and for fullerene (dash–dotted curve).

calculation yields considerably lower densities at small momenta and slightly enhanced values at large momenta compared to the FP-LMTO method. This holds for all three Cartesian momentum components of figure 4 which, according to the resulting p^2-weighting of the isotropic EMD, ensures the correct normalization for both theories. A slight asymmetry of the theoretical curves results from the pixel structure of the detector system which, of course, has been incorporated in our MC code. The comparison of the two theories in figure 3 shows that the dip in the EMD at small momenta which results from the contribution of π-electrons is more pronounced in the PP than in the FP-LMTO calculation. Smeared with resolution and multiple-scattering effects, the stronger dip yields a flatter EMD at small momenta for the PP than for the FP-LMTO calculation. It is evident from figure 4 that the FP-LMTO method describes the experimental data better than the PP method. As stated by Lou Yongming *et al* [9] the dip of the PP calculation was quite sensitive to potential parameters. They could even be adjusted in such a way that the dip completely disappeared. A slight dip in the experimental data for $\rho(0, 0, p_z)$ found in earlier $(\gamma, \mathrm{e}\gamma)$ experiments [31] could not be verified. For both calculations the LP correction has been added, though its contribution is considerably smaller than the error bars of figure 4. We emphasize that the comparison between theory and experiment in figures 4(a)–4(c) has not been done by means of a separate fit, but is the result from the global normalization described earlier.

As stated in the introduction, 2D-ACAR measures the momentum density weighted by the positron wavefunction. In a layered structure like graphite the positron localization in the interlayer region is very pronounced; see figure 1 of Puska and Nieminen [3]. Since weak interlayer bonding is primarily due to π-electrons, positron annihilation will preferentially occur with this type of electron. In figure 5 2D-ACAR measurements on highly oriented pyrolytic graphite (HOPG) [32] are compared to the angular correlation data ρ^{2D} with

$$\rho^{2D}(p_x, p_y) = \int \rho(p_x, p_y, p_z)\, \mathrm{d}p_z \tag{3}$$

from the $(\gamma, \mathrm{e}\gamma)$ experiment. It is the p character of the π-electrons which reduces the

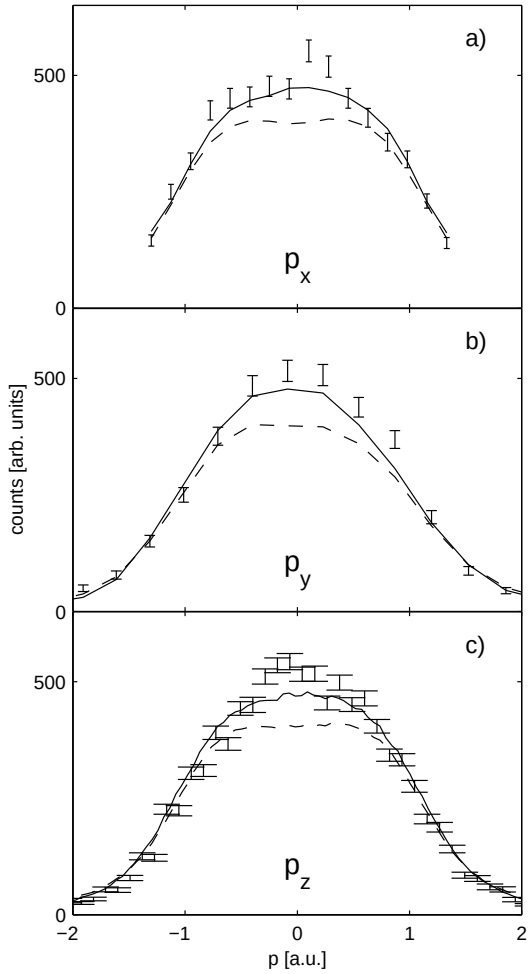

Figure 4. The experimental EMD of graphite (error bars) for the cuts $\rho(p_x, 0, 0)$ (a), $\rho(0, p_y, 0)$ (b) and $\rho(0, 0, p_z)$ (c). The solid curves show the FP-LMTO calculation and the dashed curves the PP calculation.

momentum density at small momenta. Even if the strong reduction of the ACAR density along the c-axis in HOPG were to be spherically averaged and folded with our resolution, a prominent reduction of the EMD at zero momentum would occur, in contrast to experimental observation. This clearly demonstrates the difference between the ACAR and $(\gamma, e\gamma)$ methods in investigating EMDs. In addition, one can see from figure 5 how the EMD intensity can be affected at large momenta: whereas ρ^{2D}_{ACAR} nearly vanishes for $p > 1.3$ au, the EMD from the $(\gamma, e\gamma)$ experiment still has considerable intensity; see also figure 4.

The most remarkable difference between the EMDs of graphite and C_{60} in figure 3 is the increased density of C_{60} compared to graphite at small momenta. The bending of the graphite basal planes to form the 'buckyball' induces a hybridization of wavefunctions with s character with those of the π-electrons, which results in a transfer of electron density from the interlayer region into the shell of the C_{60} spheres [33, 34]. (Nevertheless, bonding is closer to the sp^2 hybrids of graphite than to the sp^3 bonding in diamond [35].) Consequently, a

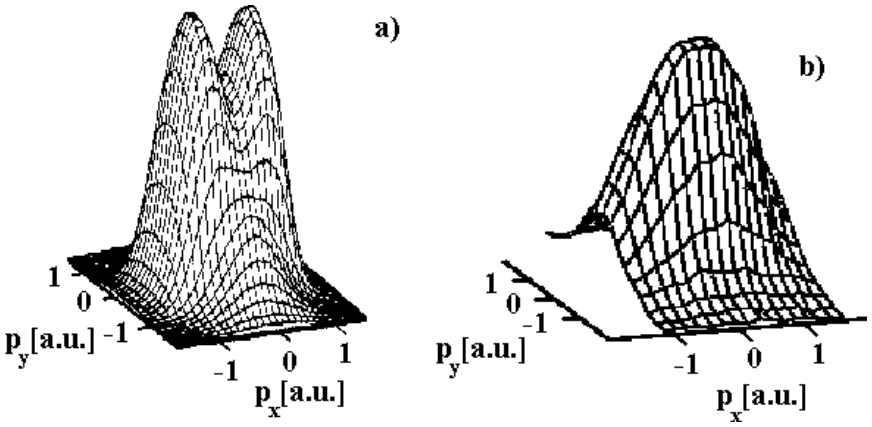

Figure 5. Angular correlation data in the case of HOPG from ACAR [32] (a) and from the (γ, eγ) experiment (b).

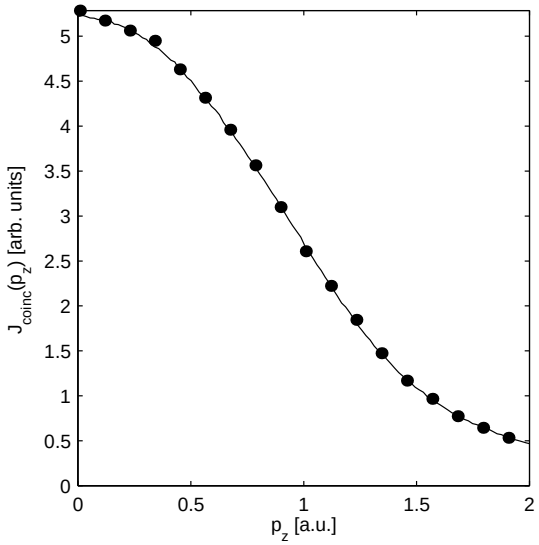

Figure 6. The experimental coincident Compton profile J_{coinc} (dots) compared to the molecular C_{60} calculation.

DFT calculation in the LDA revealed that the electron density for most of the 120 bands in fullerene showed a larger overlap among the nearest-neighbour carbon atoms in the C_{60} ball compared to graphite [17]. This kind of delocalization results apparently in an enhancement of the EMD at small momenta. A comparison of one-dimensional cuts through the EMD of fullerene with either the FP-LMTO or the molecular C_{60} calculation showed that the experiment could not distinguish between the two theories within the error bars. To improve the statistics we have summed all coincidence events for a constant p_z-value. The resulting coincident Compton profile $J_{coinc}(p_z)$ is not identical to a non-coincident one due to the limited integration range in the p_x- and p_y-directions, but besides the increase in statistics it also has the advantage that measurements in coincidence provide photon spectra free from

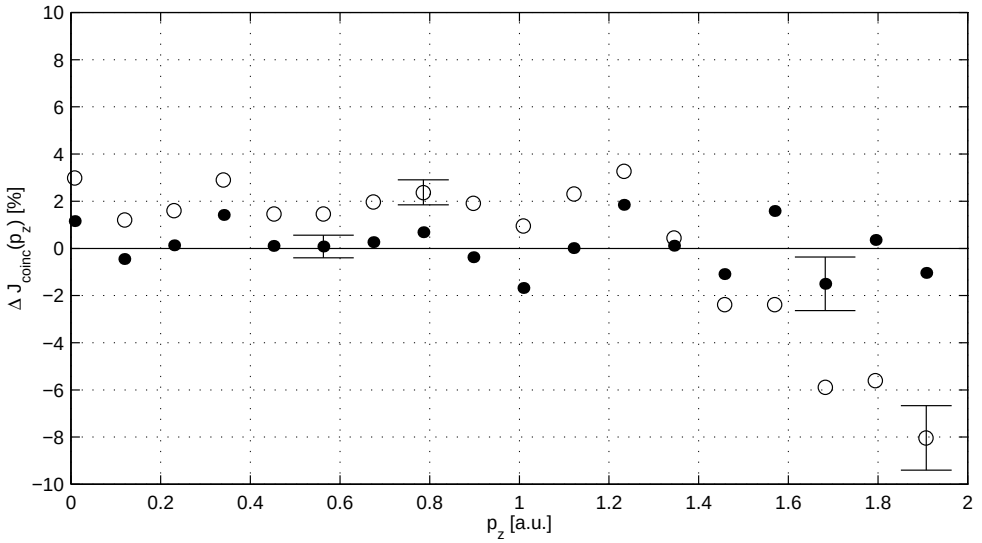

Figure 7. The relative difference ΔJ_{coinc} for the FP-LMTO calculation for graphite (open circles) and the C_{60} calculation (dots).

any background radiation. Figure 6 shows the experimental J_{coinc} as a function of p_z (data points) together with the corresponding molecular fullerite calculation. The agreement is at the percentage level. To enlarge possible differences, we have plotted in figure 7 the relative difference $\Delta J_{coinc} = (J_{exp} - J_{theor})/J_{exp} \times 100$ where J_{exp} is the experimental coincident Compton profile and J_{theor} the corresponding theoretical profile. Open circles are from the FP-LMTO calculation, while full circles represent the C_{60} calculation. Though the relative difference is rather small, the experiment clearly favours the C_{60} calculation. We mention that recent Compton profile data obtained from the measurement of the binary-encounter electron peak in 18 MeV C^{6+}/C_{60} collisions [36] did not reveal any difference between a C_{60} and a graphite Compton profile. We emphasize that the comparison of figure 7 and figure 6 relies on the fact that the graphite target, in particular, had spherically distributed crystallites. This is due to the preparation by laser ablation; evaporated films show a more HOPG-like structure [6]. This is also different from the case for macroscopic samples of graphite powder, where a strong tendency of *c*-axis orientation of the small platelets introduces a texture. It is for this reason that Moscovici *et al* [17] compared Compton profiles of fullerene with that of graphite along the *c*-axis, though about 50% of this difference is expected to be due to the anisotropy of HOPG.

5. Conclusions

We have measured the 3D electron momentum densities of graphite and fullerene. The graphite data are compared to a pseudopotential and a FP-LMTO calculation, both based on the general idea of the DFT. The FP-LMTO calculation shows better agreement with experiment, especially since it emphasizes the p-electron contribution at small momenta of the EMD less. The influence of electron correlation via a Lam–Platzman correction is discussed and found to make a negligible contribution. A comparison of the graphite and fullerene EMDs confirms a theoretical prediction of stronger electron delocalization in the ‘buckyball’ than in graphite.

Acknowledgments

The authors are grateful to Dr G Dollinger from the target laboratory of the Technische Universität München for the graphite target and Mrs D Frischke from the target laboratory of the Universität München for the fullerene target. We thank Dr M Vos from the Australian National University for making the C_{60} calculation available to us. ASK acknowledges the support from the Australian Research Council and ChM a grant from the ESRF. This work was supported by the Bundesministerium für Bildung, Wissenschaft, Forschung und Technologie, Contract Nos 05 5W MAAI and 05 ST8 HRA.

References

[1] Cooper M J 1985 *Rep. Prog. Phys.* **48** 415
[2] Riley M E, MacCallum C J and Biggs F 1975 *At. Data Nucl. Data Tables* **15** 443
[3] Puska M Y and Nieminen R M 1994 *Rev. Mod. Phys.* **66** 841
[4] Vos M, Kheifets A S, Weigold E, Canney S A and Kurp F F 1998 *J. Electron Spectrosc. Relat. Phenom.* **87** 231
[5] Suortti P and Tschentscher T 1995 *Rev. Sci. Instrum.* **66** 1798
[6] Dollinger G, Maier-Komor P and Mitwalski A 1991 *Nucl. Instrum. Methods* A **303** 79
[7] Kroto H W, Heath J R, O'Brien S C, Curl R F and Smalley R E 1985 *Nature* **318** 162
[8] Salvat F, Martinez J D, Mayol R and Parellada J 1986 *Comput. Phys. Commun.* **42** 93
[9] Lou Yongming, Johansson B and Nieminen R M 1991 *J. Phys.: Condens. Matter* **3** 1699
[10] Reed W A, Eisenberger P, Pandey K C and Snyder L C 1974 *Phys. Rev.* B **10** 1507
[11] Weyrich K H 1988 *Phys. Rev.* B **37** 10 269
[12] Skriver H L 1984 *The LMTO Method* (Berlin: Springer)
[13] Singh A K and Jarlborg T 1985 *J. Phys. F: Met. Phys.* **15** 727
[14] Glötzel D, Segall R and Andersen O K 1980 *Solid State Commun.* **36** 403
[15] Kheifets A S and Vos M 1995 *J. Phys.: Condens. Matter* **7** 3895
[16] Vos M, Canney S A, McCarthy I E, Utteridge S, Michalewicz M T and Weigold E 1997 *Phys. Rev.* B **56** 1309
[17] Moscovici J, Loupias G, Rabii S, Erwin S, Rassat A and Fabre C 1995 *Europhys. Lett.* **31** 87
[18] Bunge C F, Barrientos J A and Bunge A V 1993 *At. Data Nucl. Data Tables* **53** 113
[19] Lam L and Platzman P M 1974 *Phys. Rev.* B **9** 5122
[20] Bauer G E W 1983 *Phys. Rev.* B **27** 5912
[21] Bauer G E W and Schneider J R 1984 *Phys. Rev. Lett.* **52** 2061
[22] Lundqvist B I 1968 *Phys. Kondens. Mater.* **7** 117
[23] Tong B Y and Lam L 1978 *Phys. Rev.* A **18** 552
[24] Chen R, Trucano P and Stewart R F 1977 *Acta Crystallogr.* A **33** 823
[25] Mahaux C and Sartor 1992 *Phys. Rep.* **211** 53
[26] Farid B, Heine V, Engel G E and Robertson I J 1993 *Phys. Rev.* B **48** 11 602
[27] Schülke W, Stutz G, Wohlert F and Kaprolat A 1996 *Phys. Rev.* B **54** 12 381
[28] Moruzzi V L, Janak J F and Williams A R 1978 *Calculated Electronic Properties of Metals* (New York: Pergamon)
[29] Papanicolaou N I, Bacalis N C and Papaconstantopoulos D A 1991 *Handbook of Calculated Electron Momentum Distributions, Compton Profiles, and X-ray Form Factors of Elemental Solids* (Boca Raton, FL: CRC Press)
[30] Daniel E and Vosko S H 1960 *Phys. Rev.* **120** 2041
[31] Kurp F F, Tschentscher T, Schulte-Schrepping H, Schneider J R and Bell F 1996 *Europhys. Lett.* **35** 61
[32] Lee R R, von Stetten E C, Hasegawa M and Berko S 1987 *Phys. Rev. Lett.* **58** 2363
[33] Haddon R C 1992 *Acc. Chem. Res.* **25** 127
[34] Troullier N and Martins J L 1992 *Phys. Rev.* B **46** 1754
[35] Taylor R and Walton D R M 1993 *Nature* **363** 685
[36] DePaola B D, Parameswaran R, Walch B P, Troike M D, Richard P, Puska M Y and Nieminen R M 1995 *J. Chem. Phys.* **103** 10 413